Applied Catalysis A: General 527 (2016) 152–160

Contents lists available at ScienceDirect

Applied Catalysis A: General

journal homepage: www.elsevier.com/locate/apcata

Steam reforming of plastic pyrolysis model hydrocarbons and catalyst deactivation

Itsaso Barbarias, Gartzen Lopez, Maider Amutio, Maite Artetxe*, Jon Alvarez, Aitor Arregi, Javier Bilbao, Martin Olazar

Department of Chemical Engineering, University of the Basque Country UPV/EHU, P.O. Box 644, E48080 Bilbao, Spain

ARTICLE INFO

Article history:
Received 26 May 2016
Received in revised form 2 September 2016
Accepted 7 September 2016
Available online 9 September 2016

Keywords:
Hydrogen
Reforming
Ni catalyst
Deactivation
Coke

ABSTRACT

Catalytic steam reforming of *n*-hexane, 1-hexene, tetradecane and toluene over a Ni commercial catalyst has been carried out in a fluidized bed reactor at 700 °C. These compounds have been selected as model compounds of the volatiles formed in the pyrolysis of waste plastics in order to study in detail the performance of the catalyst in the pyrolysis-reforming of different plastic wastes. High carbon conversions and hydrogen yields are obtained at zero time on stream, with peak values being 96.5% and 82.8%, respectively, when *n*-hexane is used as model compound. Similar reactivity has been observed for tetradecane and 1-hexene, whereas lower carbon conversion (82%) and hydrogen yields (65%) are obtained for toluene. Concerning catalyst stability, olefinic compounds (1-hexene) and aromatic compounds (toluene) cause faster catalyst deactivation than paraffinic compounds (tetradecane and *n*-hexane). These disparities are explained by the different nature of the coke deposited and the different potential of the compounds to block Ni active sites, with olefins and aromatics being encapsulating coke precursors (amorphous and structured, respectively) and paraffins being filamentous and inert coke precursors.

1. Introduction

Plastic materials have contributed to the development and progress of the society for the last 150 years. The annual increase in plastic consumption has caused an increasingly environmental issue associated with their management. In 2014, 25.8 million tonnes of post-consumer plastics waste were recovered in Europe, of which 70% were treated by recycling and energy recovery processes and 30% were still land filled [1].

Among plastic waste valorisation routes, thermochemical processes have the best perspective for their large scale implantation in order to recover fuels, chemicals, monomers and H_2, with low contaminant emission [2–5]. Although gasification is the most usual process, it is generally directed to syngas production and the concentration of H_2 obtained is reduced and depends greatly on the gasifying agent used. The lower temperature used in the pyrolysis strategy improves energy efficiency of the process [6] compared to the gasification strategy. Besides, pyrolysis process is flexible and can treat mixed plastics of municipal solid waste [7], automobile recycling [8], electronics and computers [9] or construction [10].

Pyrolysis of plastic waste has been widely studied using different reactors such as batch reactors, fluidized beds, spouted beds, screw kilns and son on [11]. Fluidized beds reactors have been largely applied [12,13], but the vigorous movement of the solid in the conical spouted bed reactor (CSBR) avoids the defluidization of the bed by agglomeration of particles coated with fused plastic [14]. Moreover, pyrolysis in a CSBR was studied by feeding several plastic materials, such as polyolefins [15], PET [16], PS [17,18] and PMMA [19].

In the pyrolysis of different plastics, the circumstances and composition of the volatiles are considerably different. Thus, in the pyrolysis of polyolefins, which account for 62% of plastics in municipal solid wastes, the volatile stream is greatly dependent on pyrolysis temperature and residence time of the volatiles in the reactor. Thereby, polyolefin pyrolysis can be directed to the production of: i) waxes (low temperature and low residence time); ii) BTX aromatics (high temperature and high residence time); iii) light olefins (high temperature and low residence time) [15].

Polystyrene pyrolysis stream is mainly composed of aromatic hydrocarbons (monomer, dimer and trimer and other mono and polyaromatic hydrocarbons) and several studies have been carried out optimizing operating conditions for maximizing styrene recovery [18,20]. Regarding PET pyrolysis, the volatile stream is heterogeneous and composed of CO, CO_2, oxygenated compounds

* Corresponding author.
E-mail address: maite.artetxe@ehu.eus (M. Artetxe).

http://dx.doi.org/10.1016/j.apcata.2016.09.003
0926-860X/

and aromatics [16,21]. It should be noted that PET pyrolysis gives way to the formation of a sticky carbon residue remaining in the pyrolysis reactor.

In the production of H_2 from plastic wastes, two strategies are of interest: i) steam gasification using a reforming catalyst in situ or in-line [11,12]; ii) pyrolysis and in-line steam reforming of the hydrocarbons produced [6,22]. The products obtained in the pyrolysis-reforming strategy are greatly dependent on the intermediates formed in the first step, which are conditioned by the operating conditions, i.e., feed, catalyst used and so on [23,24]. H_2 production from HDPE pyrolysis-catalytic steam reforming was studied in a previous work [25]. HDPE pyrolysis was carried out in a CSBR and the volatiles formed were fed in-line to a fluidized bed reactor, where a Ni based commercial catalyst was placed. Under the optimum conditions, i.e., 700 °C, space time of 16.7 g_{cat} min g_{HDPE}^{-1} and steam/plastic ratio of 5, the H_2 yield was 92.5% of that corresponding to stoichometry, which accounts for a H_2 production of 38.1 g per 100 g of HDPE in the feed.

These results are encouraging, but the technological development of this strategy for plastic waste valorization involves challenges, as are: i) valorization of heterogeneous plastic wastes and ii) deactivation of the catalyst. These aspects have been approached in this paper by conducting the steam reforming of model hydrocarbons of pyrolysis volatiles corresponding to different plastics in order to ascertain the effect the type of hydrocarbon has on H_2 yield and catalyst deactivation.

In the steam reforming of fossil fuels, the catalyst is deactivated not only by coke deposition but also by sulphur poisoning and metal sintering [26–29]. In the case of hydrocarbons, the main cause of Ni based catalyst deactivation is coke deposition and three types of cokes have been distinguished, i.e., gum, whisker carbon and pyrolytic carbon [30]. Several studies focus on the influence of operating conditions and prove that coke formation is minimized by increasing reforming temperature and steam/carbon ratio [31–33]. Furthermore, the nature of the hydrocarbon in the feed has great influence on the amount and type of coke deposited [34,35].

2. Materials and methods

2.1. Model compounds

Two paraffins (*n*-hexane and tetradecane), and one olefin (1-hexene) have been chosen as model compounds for the volatile stream formed in polyolefin pyrolysis. Thus, the effect of paraffin chain length and hydrocarbon nature (olefins and paraffins) on steam reforming has been studied (reactivity at zero time on stream and catalyst deactivation by coke deposition). Besides, toluene has been used as a model compound for the aromatic compounds in the pyrolysis volatile stream, which are the main compounds in PS and PET pyrolysis.

2.2. Catalyst

The catalyst used is a commercial Ni catalyst (G90LDP catalyst) for CH_4 reforming. This catalyst was used in previous papers for hydrogen production from biomass and HDPE pyrolysis-reforming [25,36]. The catalyst has been supplied by Süd Chemie and its chemical formulation is based on NiO (14 wt.%), $CaAl_3O_4$ and Al_2O_3. This catalyst was ground and sieved to 0.4–0.8 mm and, prior to the reforming reaction, has been subjected to an in situ reduction process at 710 °C for 4 h under a 10 vol.% H_2 stream in order to ensure complete reduction of NiO.

Table 1 shows the metal content and physical properties of the catalyst. The physical properties have been measured by N_2 adsorption-desorption (Micromeritics ASAP 2010). The temperature programmed reduction (TPR) of the catalyst has been measured by AutoChem II 2920 Micromeritics [37], which enables to establish the catalyst reduction temperature prior to use.

Table 1
Metal content and physical properties of the catalyst.

Catalyst	NiO content, wt.%	S_{BET}, $m^2\ g^{-1}$	V_{pore}, $cm^3\ g^{-1}$	d_{pore}, Å
G90LDP	14	19	0.04	122

2.3. Experimental equipment and conditions

A scheme of the bench-scale unit used for model compound catalytic steam reforming is shown in Fig. 1. The reforming reaction has been carried out in a fluidized bed reactor with an internal diameter of 38.1 mm and a total length of 440 mm. This reactor is located inside a 550 W radiant oven which provides the energy needed to maintain the reaction temperature, which is controlled by a thermocouple placed in the catalyst bed. The effect of the operating conditions in the reforming reactor was studied in a previous paper, in which HDPE pyrolysis volatiles were reformed in a fluidized bed reactor [25]. Thus, a reforming temperature of 700 °C has been chosen in order to obtain a high conversion of model compounds and avoid irreversible deactivation of Ni catalyst by sintering.

The catalyst mass used was 7.5 g, corresponding to a space time of 10 $g_{catalyst}$ min $g_{compound}^{-1}$. Sand was used as an inert material to obtain a catalytic bed of 25 g. The particle size of the catalyst was 0.4-0.8 mm and that of the inert sand 0.3–0.35 mm, which were determined in a previous hydrodynamic as suitable sizes to ensure a good performance in the reactor.

In order to avoid the condensation of steam, model compounds and the volatile stream formed, the reactor is located within a forced convection oven maintained at 270 °C. Moreover, inside the forced convection oven a sintered steel filter (5 μm) is located with the aim of recovering elutriated catalyst fines from the reactor.

Water and the model compounds are separately pumped into the preheater at room temperature with constant pumping flow rate. The model compounds are continuously fed by means of a PHD 4400 pump and have been vaporized using an electric cartridge placed outside the forced convection oven. The model compounds used have been *n*-hexane, 1-hexene and toluene purchased from Merck Millipore and tetradecane from Acros Organics. The model compound flow rate has been 0.75 g min^{-1}.

Water has been fed by means of a Gilson 307 pump and vaporized using an electric cartridge placed outside the forced convection oven. The water flow rate used has been 3 mL min^{-1}, corresponding to a steam flow rate of 3.73 NL min^{-1} and a steam/feedstock ratio of 4. The vaporized model compounds and steam are mixed and jointly fed into the reforming reactor. Moreover, N_2 is used as fluidizing agent during the heating process preceding the reaction.

The volatile stream formed in the reforming reactor circulate through a condensation system consisting of a condenser (cooled with tap water), a peltier and a coalescence filter, which ensure the total condensation and retention of the non-reacted steam and model compound derived products.

Experiments at zero time on stream have been repeated at least 3 times to ensure reproducibility of the results and the mass balance closure was between 95% and 105% in all runs.

2.4. Product analysis

As shown in Fig. 1, the volatile stream leaving the reforming reactor has been analysed on-line by means of a GC Varian 3900 provided with and HP-Pona column and a flame ionization detector (FID). The sample has been injected into the GC prior to condensation by means of a line thermostated at 280 °C in order

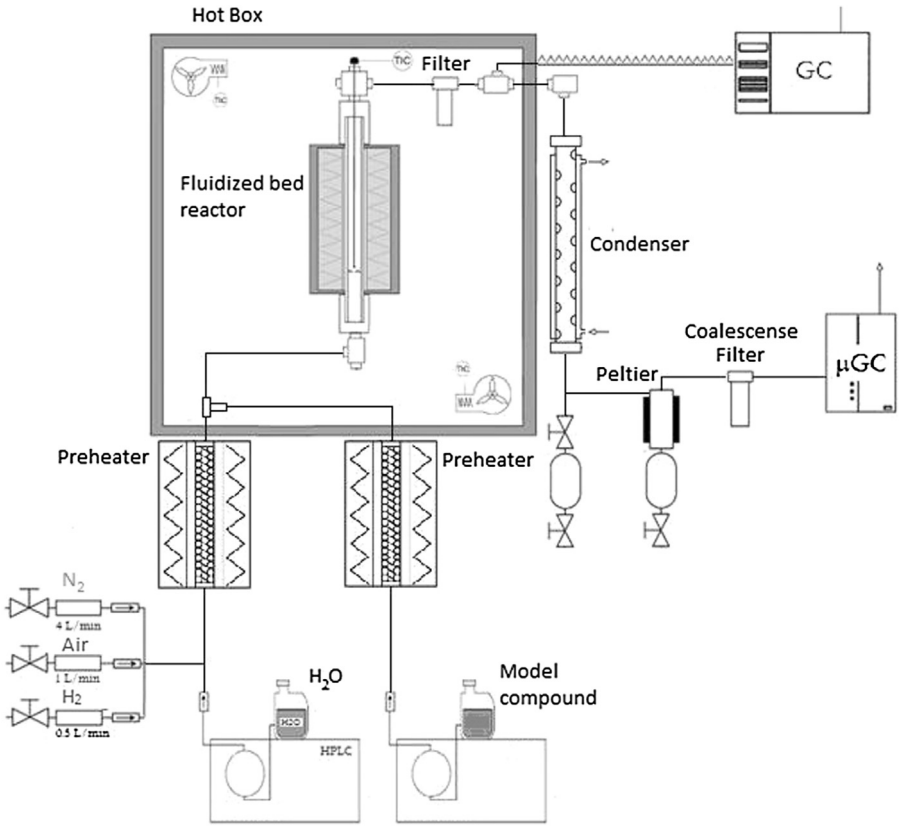

Fig. 1. Scheme of the laboratory scale catalytic steam reforming plant.

to avoid the condensation of heavy hydrocarbon compounds. The non-condensable gases leaving the condensation system (ensures total condensation of volatile hydrocarbons) have been analysed on-line in a micro GC (Varian 4900). This product analysis allows a detailed quantification of the whole product stream.

The amount of coke deposited on the used catalysts has been measured by temperature programmed oxidation (TPO), in a thermobalance (TGA Q5000TA Thermo Scientific), connected on-line to a Blazer Instruments mass Spectrometer (Thermostar), according to the following procedure: (i) signal stabilization with He stream at 100 °C for 30 min, (ii) a ramp of 5 °C min^{-1} to 800 °C in a stream of O_2 diluted in He, with this temperature remaining constant for 30 min in order to ensure full coke combustion. The nature of the coke deposited on the catalyst has been studied by TEM (transmission electron microscopy) images and SEM (scanning electron microscopy) images, obtained by means of Phillips CM20 and JEOL JSM-6400, respectively.

2.5. Reaction indexes

In order to quantify the process results, the following reaction indexes have been defined: i) model compound conversion (carbon conversion efficiency), i.e., the moles of C recovered in the gaseous stream as CO_2 and CO over those fed in the model hydrocarbon:

$$X = \frac{C_{Gas(CO+CO_2)}}{C_{hydrocarbon}} 100 \quad (1)$$

The moles of C converted to other gaseous compounds (CH_4 and C_2–C_4 hydrocarbons) have not been included because these compounds are formed by cracking reactions. In fact, its inclusion would mask the real conversion of the hydrocarbons to reforming products.

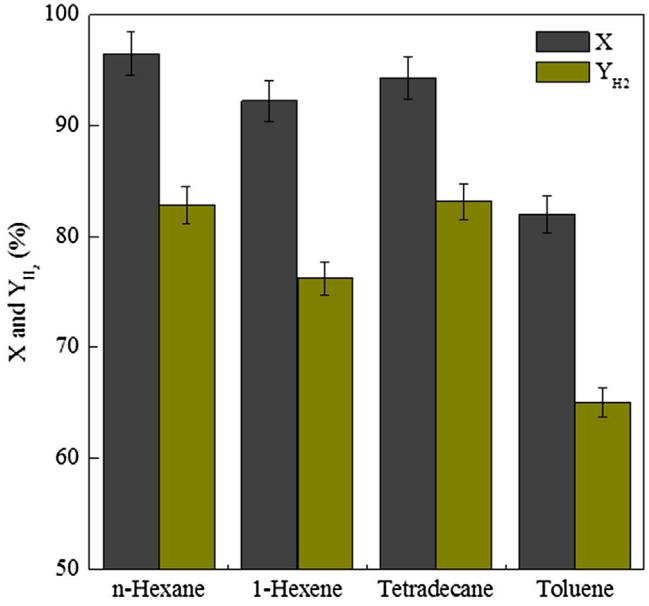

Fig. 2. Conversions and H_2 yields obtained with each model compound.

ii) The yields of individual products based on the model hydrocarbon in the feed:

$$Y_i = \frac{F_i}{F_{hydrocarbon}} 100 \quad (2)$$

where F_i and $F_{hydrocarbon}$ are the molar flow rates of i product and model hydrocarbon given in C moles, respectively.

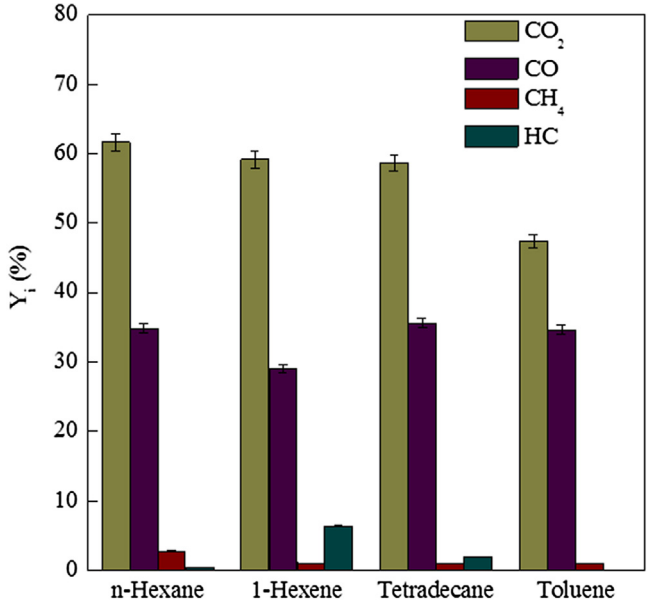

Fig. 3. CO_2, CO, CH_4 and other gaseous hydrocarbon yields obtained with each model compound.

iii) Hydrogen yield given as a percentage of the maximum allowed by stoichiometry, Eq. (3), according to the stoichiometry in Eq. (4):

$$Y_{H_2} = \frac{F_{H_2}}{F^0_{H_2}} 100 \quad (3)$$

where F_{H2} and F^0_{H2} are the actual molar flow rate of hydrogen and the maximum corresponding to stoichiometry, respectively.

$$C_nH_m + 2nH_2O \rightarrow nCO_2 + \left(2n + m/2\right) H_2 \quad (4)$$

3. Results

3.1. Conversion of the model compounds

Fig. 2 displays the conversion and H_2 yield obtained in the reforming of each model compound at zero time on stream. It can be observed that high carbon conversions (higher than 92%) are obtained for *n*-hexane, 1-hexene and tetradecane, whereas carbon conversion is lower (82%) for toluene. It is well-known that aromatic compounds are less reactive than linear hydrocarbons, which is attributed to a higher C—C bond energy of the aromatic hydrocarbons [38].

In order to ascertain the products in Fig. 2, the following reaction have been considered:

$$\text{Hydrocarbon steam reforming}: \ C_nH_m + nH_2O \rightarrow nCO + \left(n + m/2\right) H_2 \quad (5)$$

$$\text{Water gas shift}\,(WGS): \ CO + H_2O \Leftrightarrow CO_2 + H_2 \quad (6)$$

$$\text{Methane steam reforming}: \ CH_4 + H_2O \Leftrightarrow CO + 3H_2 \quad (7)$$

$$\text{Cracking (secondary reaction)}: \ C_nH_m \rightarrow \text{paraffins} + \text{olefins} \quad (8)$$

Regarding linear hydrocarbons, although high conversions are observed for all compounds, small differences can be observed depending on the chain length and the paraffinic or olefinic nature of the hydrocarbon. Thus, as the carbon atom number of the paraffin is higher, the conversion observed is lower (97% for *n*-hexane and 94% for tetradecane), which is explained by the slower reaction kinetics of long-chain hydrocarbons. Furthermore, although the same mass flow rate is in the feed for both compounds, the partial pressure of *n*-hexane is higher than that of tetradecane, which also enhances reaction kinetics. Reforming reactions take place by irreversible adsorption of the hydrocarbons on the nickel surface and the subsequent breakage of terminal C—C bonds until the hydrocarbon is converted into C_1 hydrocarbon [39]. Thus, as the chain length of the hydrocarbons is higher, the reforming rate is lower. According to the nature of the hydrocarbons, 1-hexene conversion (92%) is lower than that of *n*-hexane (97%) because olefins are more liable to thermal cracking than paraffins. Above 600–650 °C, thermal cracking reactions begin to compete with steam reforming reactions [39], and therefore a lower reforming reaction rate is observed for 1-hexene.

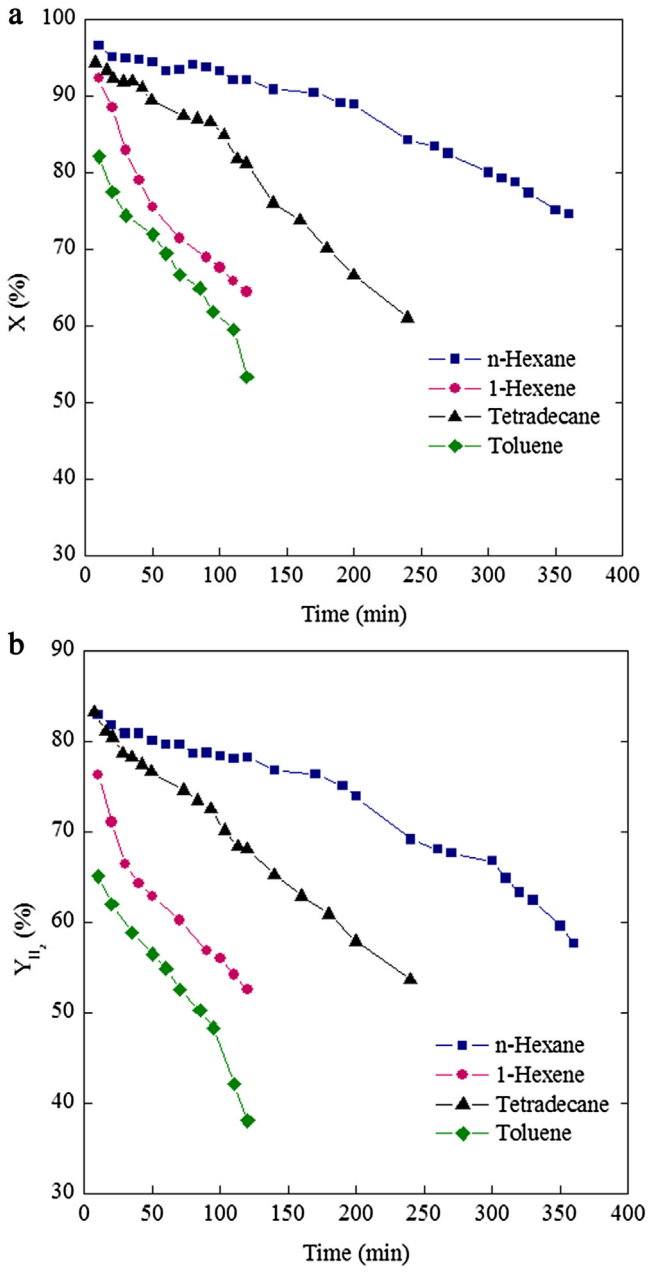

Fig. 4. Effect of time on stream on conversions (a) and H_2 yields (b).

Regarding the H_2 yield obtained in the steam reforming of different model hydrocarbons, similar trends are observed, with the H_2 yield obtained for linear hydrocarbons (>76%) being higher than that obtained for toluene (65%). Furthermore, although lin-

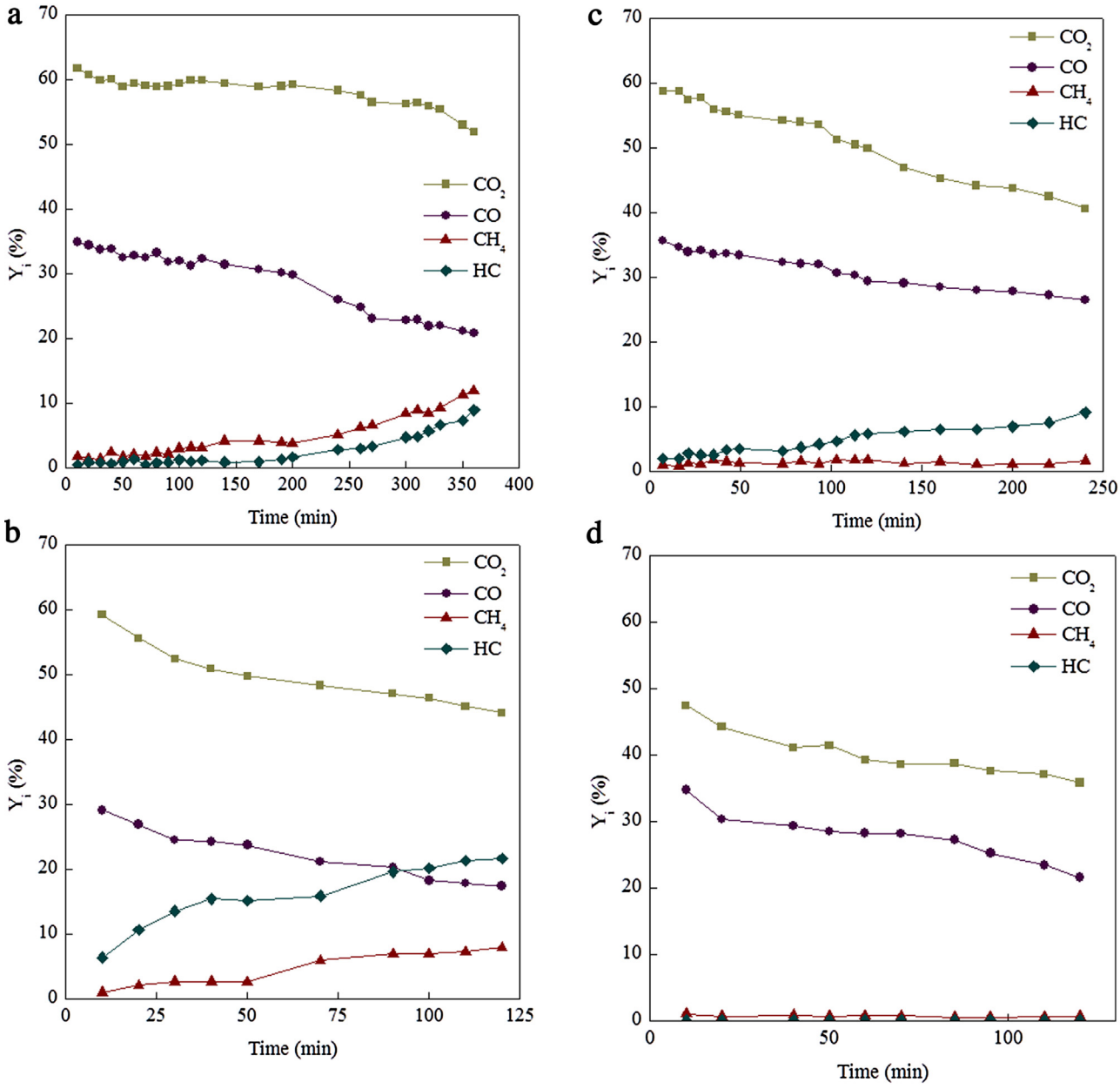

Fig. 5. Effect of time on stream on the remaining gaseous product yields in the reforming of *n*-hexane (a), 1-hexene (b), tetradecane (c) and toluene (d).

ear hydrocarbons undergo similar conversion, with the one for 1-hexene being slightly lower, the difference between the H_2 yield obtained for 1-hexene (76%) and *n*-hexane (83%) is more pronounced. Nevertheless, a comparison based on the carbon atom number does not seem to reveal significant differences in the H_2 yield obtained.

It should be noted that, apart from the different reactivity of the compounds, the carbon content per mass unit of the different compounds may have an influence on the conversions and H_2 yields observed. The space time used in all runs is the same ($10\,g_{cat}\,min\,g_{m.compound}^{-1}$), but the effective space time used (grams of catalyst per carbon flow rate) is not the same. Thereby, the effective space time used is as follows, according to a decreasing order: *n*-hexane > n-hexene > tetradecane > toluene. Therefore, the lower carbon conversion observed for toluene compared to linear hydrocarbons, as well as for tetradecane compared to *n*-hexane, is also a consequence of the lower effective space-time used with these compounds.

Fig. 3 shows CO_2, CO, CH_4 and other gaseous hydrocarbon yields obtained in the steam reforming of the model compounds. The results obtained confirm the trend observed for conversion and H_2 yield. A comparison of linear hydrocarbons with toluene shows that a lower CO_2 yield is observed for toluene (59–62% for linear hydrocarbons and 47% for toluene), which is a consequence of the poorer reactivity of aromatic hydrocarbons. Regarding linear hydrocarbons, a lower CO yield (29%) is obtained for 1-hexene compared to the two paraffins (35%). This effect is explained by the higher cracking reactivity of olefins compared to paraffins and the lower reforming rate due to the competence of both reactions at reforming temperatures. The higher hydrocarbon yields obtained with 1-hexene (6%), insignificant for *n*-hexane, indicate that cracking reactions take place more extensively for olefins.

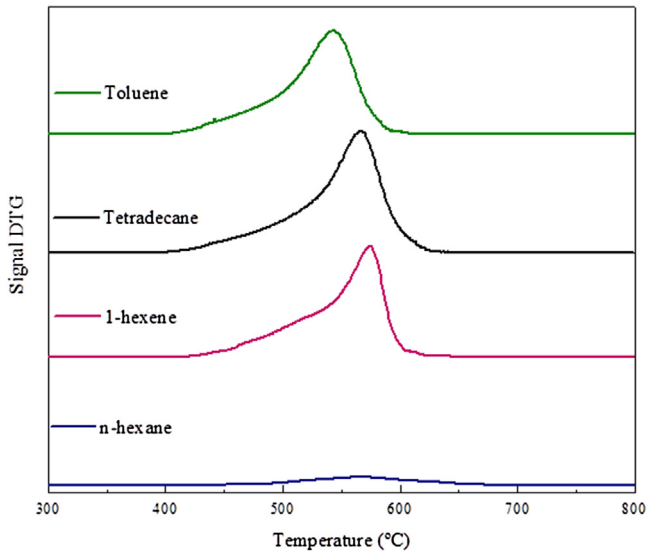

Fig. 6. TPO curves of the coke deposited on the catalyst in the reforming of *n*-hexane, 1-hexene, tetradecane and toluene.

3.2. Catalyst stability

Fig. 4 shows the evolution of conversions (Fig. 4a) and H_2 yields (Fig. 4b) with time on stream for different model compounds. The results obtained reveal the significant effect of the composition in the reaction medium on catalyst stability. Thus, the following order of catalyst deactivation rate is observed: toluene > 1-hexene > tetradecane > n-hexane. The main cause of Ni catalyst deactivation is coke deposition, in which carbon is deposited on the catalyst surface, hindering contact between reactants and the catalyst active sites and decreasing the reforming reaction rate. Coke formation and its evolution throughout reforming takes place by the contribution of the following steps [40,41]:

Olefin polymerisation :

$$nC_2H_4 \rightarrow \text{oligomers} \rightarrow \text{encapsulanting coke} \rightarrow \text{filamentous coke} \quad (9)$$

$$\text{Dehydrogenation of methane} : CH_4 \leftrightarrow C\,(\text{filamentous coke}) + 2H_2 \quad (10)$$

$$\text{Boudouard reaction} : 2CO \leftrightarrow C\,(\text{filamentous coke}) + CO_2 \quad (11)$$

Aromatic polycondensation :

$$\text{Aromatics} \rightarrow \text{polyaromatics} \rightarrow \text{highly structured coke} \quad (12)$$

In order to explain the effect of the hydrocarbon type on the catalyst deactivation rate, the difference in the distribution of byproducts (Fig. 3) and their role as precursors for coke formation (Eqs. (9)–(12)) should be considered. Furthermore, catalyst deactivation is attributed mainly to the blockage of Ni active sites by the adsorbed coke (mainly amorphous coke), whereas filamentous coke contributes to a lesser extent to deactivation because it has minor relation with Ni active sites and grows towards the outside of catalyst particles [40,41].

Although 1-hexene leads to high conversion and H_2 yield at zero time of stream, a fast deactivation rate is observed (Fig. 4). Thus, carbon conversion and H_2 yield decrease from 92% and 76% at zero time on stream to 64% and 53% for 120 min, respectively.

The fast deactivation observed in 1-hexene reforming (Fig. 4) is consistent with the coke formation role of light olefins (especially ethylene), which are obtained by cracking reactions and are considered the main coke precursors, with high oligomerization activity to form firstly encapsulating coke and then evolve to filamentous coke (Eq. (9)) [42].

Fast catalyst deactivation is also observed when toluene is used as model compound (conversion and H_2 yield decrease from 82% and 65% to 53% and 38% for 120 min), which evidences the trend of aromatic compounds to form coke (Eq. (12)). Apart from the high capability of aromatic compounds to condense and form coke [43–45], the low reactivity of these compounds enhances coke formation. Thereby, as more coke is formed, catalyst activity is lower and coke formation rate is higher.

Furthermore, Fig. 4 shows that paraffin chain length has a significant effect on catalyst deactivation rate. Although *n*-hexane and tetradecane have similar conversion at zero time on stream, catalyst deactivation is more pronounced for tetradecane, for which conversion decrease from 94% to 61% for 240 min, whereas for *n*-hexane conversion decrease from 97% to 75% for 360 min. As aforementioned, thermal cracking at the reforming temperatures competes with reforming reactions, with the reaction rate for the latter being lower for long chain hydrocarbons [19]. Therefore, more thermal cracking products (CH_4, light hydrocarbons and so on) are formed for tetradecane, which are coke precursors and responsible for a faster catalyst deactivation (Eq. (8)). Moreover, an autocatalytic effect is observed due to the enhancement of thermal cracking reactions when the catalyst is being deactivated, i.e., a higher concentration of coke precursors (especially CH_4) in the reaction medium and so a faster catalyst deactivation.

Fig. 5 shows the evolution of gaseous products yields with time on stream for *n*-hexane (Fig. 5a), 1-hexene (Fig. 5b), tetradecane (Fig. 5c) and toluene (Fig. 5d). Considerable differences in the evolution of gaseous products are observed in the reforming of these model hydrocarbons.

A low deactivation rate is observed for *n*-hexane reforming at low times on stream (Fig. 5a), for which the yields of CO (32%) and CO_2 (59%) are almost constant until 120 min, with CH_4 and light hydrocarbon yields being almost insignificant. As time on stream is increased the yield of CO_2 and CO decreases due to coke deposition on the catalyst, which lowers catalyst activity and increases the yield of CH_4 and light hydrocarbons (thermal cracking products). Catalyst deactivation rate increases with time on stream due to the increase in CH_4 and light hydrocarbon concentrations in the reaction medium, which affects more significantly the reforming reaction than the water gas shift reaction and so decreases preferentially the yield of CO.

Regarding the evolution of gaseous product yields in 1-hexene reforming (Fig. 5b), high deactivation rate is observed at a low time on stream due to high CH_4 and light hydrocarbon yields even at zero time on stream. The presence of these coke precursors in the reaction medium causes a sharp decrease in CO and CO_2 yield, from 29% and 59% at zero time on stream to 17% and 44% for 120 min, respectively. This similar decrease in CO and CO_2 yields evidences that catalyst deactivation has the same influence on reforming and water gas shift reactions. Besides, given that deactivation affects reforming and water gas shift reactions, thermal cracking reactions are enhanced and a significant increase in CH_4 and light hydrocarbon yields is observed with time on stream, reaching a value of 8% and 22%, respectively, for 120 min.

Tetradecane (Fig. 5c) shows an intermediate trend between *n*-hexane and 1-hexene, with catalyst deactivation rate being faster than for *n*-hexane reforming and lower than for 1-hexene reforming. When the catalyst is deactivated, CO and CO_2 yields decrease to 26% and 41%, respectively, for 240 min, and therefore the yield of light hydrocarbons increases, reaching 9%. An autocatalytic effect

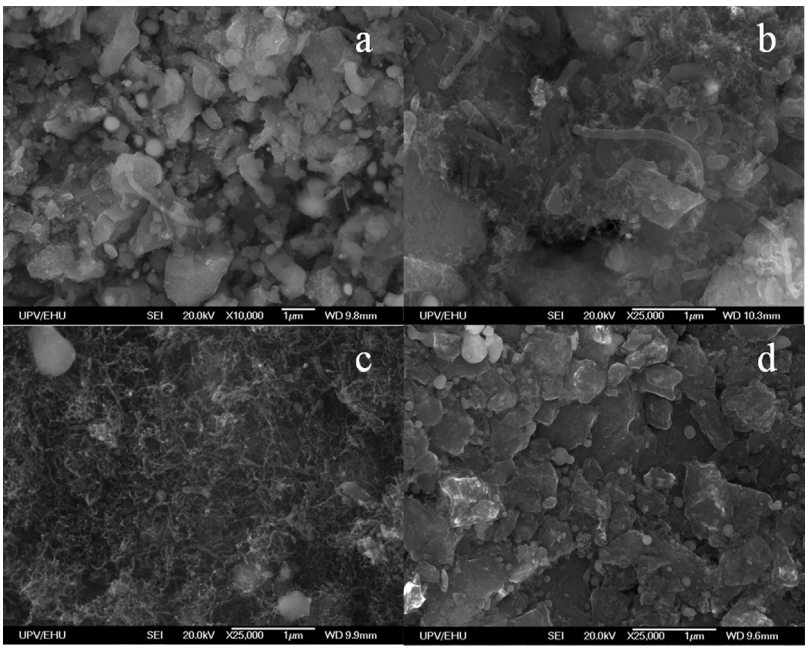

Fig. 7. SEM images of the coke deposited on the catalyst in the reforming of *n*-hexane (a), 1-hexene (b), tetradecane (c) and toluene (d).

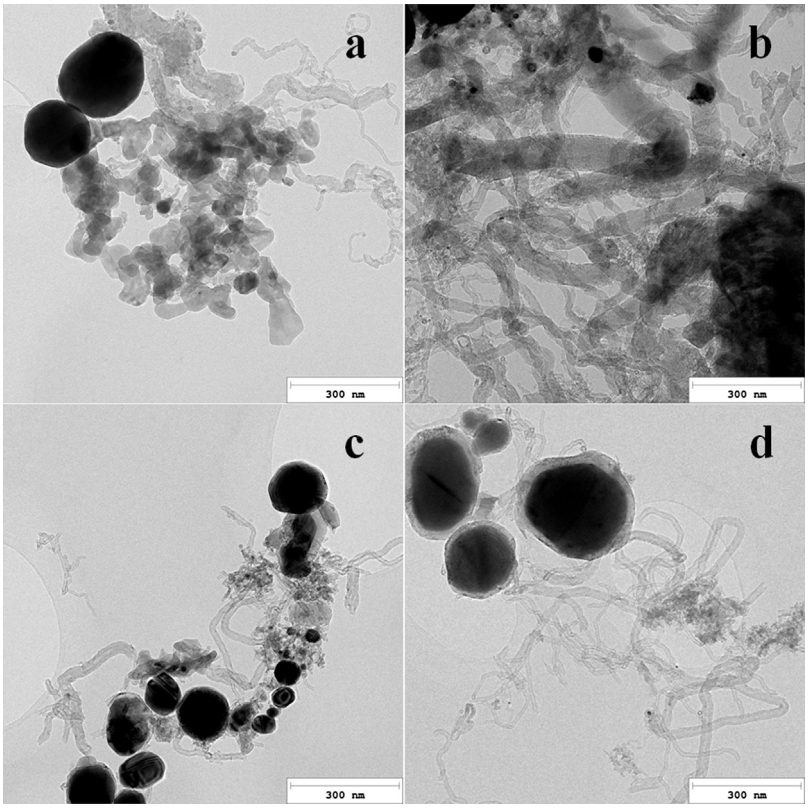

Fig. 8. TEM images of the coke deposited on the catalyst in the reforming of *n*-hexane (a), 1-hexene (b), tetradecane (c) and toluene (d).

is observed, with deactivation rate being faster as time on stream is increased, which is due to an increase in coke precursor concentration in the reaction medium.

According to the evolution of gaseous product yields with time on stream in toluene reforming (Fig. 5d), a sharp decrease in CO and CO_2 yield is observed as time on stream is increased, from 35% and 47% at zero time on stream to 22% and 36% for 120 min, respectively. However, neither CH_4 nor light hydrocarbons are formed due to the low cracking reactivity of aromatic compounds [42], i.e., their yield is insignificant even for 120 min. Therefore, the fast deactivation rate observed for toluene is caused by the coke deposited from non-reformed aromatic compound condensation [43–45].

3.3. Characterization of the coke deposited

In order to analyze the amount and nature of the coke deposited on the catalyst in the reforming of different model hydrocarbons and its effect on catalyst deactivation, temperature programmed oxidation (TPO) of the coke deposited on the deactivated catalyst has been carried out. As observed in Fig. 6, TPO profiles show great differences. Thus, the coke amounts deposited for *n*-hexane, tetradecane, 1-hexene and toluene are as follows: 1.65% g_{cat}^{-1} for 360 min, 16.15% g_{cat}^{-1} for 240 min, 13.00% g_{cat}^{-1} for 120 min and 13.70% g_{cat}^{-1} for 120 min, respectively.

Apart from the differences observed in the coke amount deposited, it is also observed that the nature of the coke deposited on the catalyst varies depending on the model compound used. A prevailing peak is observed at 570 °C for *n*-hexane, tetradecane and 1-hexene, which is related to the combustion of the filamentous carbon formed by evolution of the amorphous coke (Eq. (9)), methane dehydrogenation (Eq. (10)) and Boudouard reaction (Eq. (11)) [32,46,47]. Besides, a significant shoulder is observed at lower temperatures (450 °C) indicating the combustion of amorphous carbon formed preferably by olefin polymerization (Eq. (9)) [46,48–50]. As observed, the peak related to the filamentous carbon is higher for tetradecane than for 1-hexene, whereas that for amorphous carbon is higher for 1-hexene. Thus, the faster catalyst deactivation observed for 1-hexene should be attributed mainly to the amorphous coke deposited on Ni active sites, which causes their blockage. According to the coke deposited in toluene reforming, its combustion shows a main peak at 540 °C, indicating the different nature of the coke formed from aromatic compounds by their polymerization and condensation reactions (Eq. (12)).

Fig. 7 shows SEM images for the catalysts deactivated in the reforming of *n*-hexane (a), 1-hexene (b), tetradecane (c) and toluene (d). As observed, although some fibres are formed in the case of 1-hexene, mainly amorphous coke is deposited on the catalyst surface. However, the coke deposited in the steam reforming of tetradecane is mainly filamentous coke, which is not deposited on the Ni active sites and so its deactivating effect is not as severe as that of the amorphous coke [51]. Concerning the coke formed in toluene reforming, it is not filamentous coke. The higher combustion temperature of this coke ascertained from the TPO analyses is related to a more structured coke formed from aromatic compounds, whose combustion requires higher temperatures, even though it is deposited close to combustion activating Ni active sites.

Fig. 8 shows TEM images for the catalysts deactivated in the reforming of *n*-hexane (a), 1-hexene (b), tetradecane (c) and toluene (d). Consistent with SEM images, the reforming of the olefinic compound leads mainly to the formation and deposition of amorphous carbon, which is responsible for the fast deactivation of the catalyst. Nevertheless, reforming of paraffins leads mainly to filamentous coke, whose effect on catalyst activity is not as pronounced as amorphous coke because it is not deposited on Ni active sites. Regarding toluene reforming, the coke formed is not of filamentous structure so its high combustion temperature should be attributed to the highly structured nature of the coke formed from aromatic polymerization and condensation reactions. Based on the fast deactivation observed in toluene reforming, this condensed coke has a high capacity for blocking Ni sites because it is not a filamentous matter growing towards the outside of the catalyst particles.

4. Conclusions

Steam reforming of different model compounds (*n*-hexane, 1-hexene, tetradecane and toluene), representative of plastic pyrolysis volatiles, has shown that the composition in the reaction medium has great influence not only on the conversion and H_2 yield obtained at zero time on stream but also on the amount and nature of the coke formed, and therefore on catalyst deactivation.

Although slight differences are observed, high carbon conversion and H_2 yields are obtained at zero time on stream (>92% and >76%, respectively) for linear hydrocarbons. As the paraffin molecule is longer the reforming rate is lower, but a comparison of the paraffin (*n*-hexane) with the olefin (1-hexene) shows that olefin susceptibility to thermal cracking leads to a decrease in the reforming reaction rate. Besides, lower conversion and H_2 yield is observed for toluene, 82% and 65%, respectively, which evidences a lower reactivity of aromatic hydrocarbons compared to linear hydrocarbons.

Catalyst deactivation is highly dependent on the composition in the reaction medium due to its effect on the nature of the coke. The presence of light olefins leads to the formation of amorphous carbon, which is deposited on Ni active sites and causes fast catalyst deactivation. Thus, the high amount of light olefins in 1-hexene reforming due to its thermal cracking causes faster catalyst deactivation than in paraffin reforming. Furthermore, as the paraffin molecule is longer, the reforming rate of the compound is lower and the thermal cracking rate is higher, with the latter leading to products causing catalyst deactivation. These products form preferably filamentous carbon, which is not deposited on Ni active sites, and therefore cause slow catalyst deactivation. Besides, aromatic compounds have high capability for condensing and forming a structured coke deposited on the catalyst surface, which is responsible for fast catalyst deactivation.

Acknowledgments

This work was carried out with financial support from the Ministry of Economy and Competitiveness of the Spanish Government (CTQ2013-45105-R and CTQ2014-59574-JIN), The EDRF funds, the Basque Government (IT748-13) and the University of the Basque Country (UFI 11/39).

References

[1] Plastics, Plastics Europe, Plastics-the Facts, 2014–15; An Analysis of European plastics production, demand and waste data (2015).
[2] S.M. Al-Salem, P. Lettieri, J. Baeyens, Prog. Energy Combust. 36 (2010) 103–129.
[3] U. Arena, L. Zaccariello, M.L. Mastellone, Waste Manage. 29 (2009) 783–791.
[4] P.J. Donaj, W. Kaminsky, F. Buzeto, W. Yang, Waste Manage. 32 (2012) 840–846.
[5] A. Angyal, N. Miskolczi, L. Bartha, J. Anal. Appl. Pyrolysis 79 (2004) 409–414.
[6] T. Namioka, A. Saito, Y. Inoue, Y. Park, T. Min, S. Roh, Appl. Energy 88 (2011) 2019–2026.
[7] G. López, M. Olazar, R. Aguado, J. Bilbao, Fuel 89 (2010) 1946–1952.
[8] I. de Marco, B.M. Caballero, M.A. Cabrero, M.F. Laresgoiti, A. Torres, M.J. Chomón, J. Anal. Appl. Pyrolysis 79 (2007) 403–408.
[9] Q. Guo, X. Yue, M. Wang, Y. Liu, Powder Technol. 198 (2010) 422–428.
[10] B. Kang, S.G. Kim, J. Kim, J. Anal. Appl. Pyrolysis 81 (2008) 7–13.
[11] S.L. Wong, N. Ngadi, T.A.T. Abdullah, I.M. Inuwa, Renew. Sustain. Energy Rev. 50 (2015) 1167–1180.
[12] J.A. Conesa, R. Font, A. Marcilla, A.N. Garcia, Energy Fuels 8 (1994) 1238–1246.
[13] W. Kaminsky, M. Predel, A. Sadiki, Polym. Degrad. Stab. 85 (2004) 1045–1050.
[14] R. Aguado, M.J. San Jose, M. Olazar, S. Alvarez, J. Bilbao, Chem. Eng. Process. 44 (2005) 231–235.
[15] G. Elordi, M. Olazar, G. Lopez, M. Artetxe, J. Bilbao, Ind. Eng. Chem. Res. 50 (2011) 6650–6659.
[16] M. Artetxe, G. Lopez, M. Amutio, G. Elordi, M. Olazar, J. Bilbao, Ind. Eng. Chem. Res. 49 (2010) 2064–2069.
[17] R. Aguado, M. Olazar, B. Gaisán, R. Prieto, J. Bilbao, Chem. Eng. J. 92 (2003) 91–99.
[18] M. Artetxe, G. Lopez, M. Amutio, I. Barbarias, A. Arregi, R. Aguado, J. Bilbao, M. Olazar, Waste Manage. 45 (2015) 126–133.
[19] G. Lopez, M. Artetxe, M. Amutio, G. Elordi, R. Aguado, M. Olazar, Chem. Eng. Process. 49 (2010) 1089–1094.
[20] Y. Liu, J. Qian, J. Wang, Fuel Process. Technol. 63 (2000) 45–55.
[21] T. Yoshioka, G. Grause, C. Eger, W. Kaminsky, A. Okuwaki, Polym. Degrad. Stab. 86 (2004) 499–504.
[22] S. Czernik, R.J. French, Energy Fuels 20 (2006) 754–758.

[23] W.W. Liu, C.W. Hu, D.M. Tong, Y. Yang, G.Y. Li, L.F. Zhu, J.Q. Tang, Energy Convers. Manage. 88 (2014) 565–572.
[24] W.W. Liu, C.W. Hu, Y. Yang, D.M. Tong, L.F. Zhu, R.N. Zhang, B.H. Zhao, Appl. Catal. B—Environ. 129 (2013) 202–213.
[25] I. Barbarias, G. Lopez, J. Alvarez, M. Artetxe, A. Arregi, J. Bilbao, M. Olazar, Chem. Eng. J. 296 (2016) 191–198.
[26] C. Fauteux-Lefebvre, N. Abatzoglou, N. Braidy, I.E. Achouri, J. Power Sources 196 (2011) 7673–7680.
[27] F. Morales-Cano, L.F. Lundegaard, R.R. Tiruvalam, H. Falsing, M.S. Skjøth-Rasmussen, Appl. Catal. A—Gen. 498 (2015) 117–125.
[28] C.P.B. Quitete, R.C.P. Bittencourt, M.M.V.M. Souza, Appl. Catal. A—Gen. 478 (2014) 234–240.
[29] C.H. Bartholomew, Appl. Catal. A—Gen. 212 (2001) 17–60.
[30] J.R. Rostrup-Nielsen, Catalysis, Science and Engineering, second ed., Springer, Berlin, 1984.
[31] J.C. Acomb, C. Wu, P.T. Williams, Appl. Catal. B—Environ. 147 (2014) 571–584.
[32] A. Remiro, B. Valle, A.T. Aguayo, J. Bilbao, A.G. Gayubo, Fuel Process. Technol. 115 (2013) 222–232.
[33] G.T. Wurzler, R.C. Rabelo-Neto, L.V. Mattos, M.A. Fraga, F.B. Noronha, Appl. Catal. A—Gen. 518 (2016) 115–128.
[34] T. Sperle, D. Chen, R. Lødeng, A. Holmen, Appl. Catal. A—Gen. 282 (2005) 195–204.
[35] O. Sidjabat, D.L. Trimm, Top. Catal. 11–12 (2000) 279–282.
[36] A. Arregi, G. Lopez, M. Amutio, I. Barbarias, J. Bilbao, M. Olazar, RSC Adv. 6 (2016) 25975–25985.
[37] A. Erkiaga, G. Lopez, I. Barbarias, M. Artetxe, M. Amutio, J. Bilbao, M. Olazar, J. Anal. Appl. Pyrolysis 116 (2015) 34–41.
[38] K. Murata, L. Wang, M. Saito, M. Inaba, I. Takahara, N. Mimura, Energy Fuels 18 (2004) 122–126.
[39] F. Joensen, J.R. Rostrup-Nielsen, J. Power Sources 105 (2002) 195–201.
[40] J. Vicente, C. Montero, J. Ereña, M.J. Azkoiti, J. Bilbao, A.G. Gayubo, Int. J. Hydrogen Energy 39 (2014) 12586–12596.
[41] C. Montero, A. Ochoa, P. Castaño, J. Bilbao, A.G. Gayubo, J. Catal. 331 (2015) 181–192.
[42] J.R. Rostrup-Nielsen, D.L. Trimm, J. Catal. 48 (1977) 155–165.
[43] D. Shekhawat, T.H. Gardner, D.A. Berry, M. Salazar, D.J. Haynes, J.J. Spivey, Appl. Catal. A—Gen. 311 (2006) 8–16.
[44] K.M. Hardiman, C.G. Cooper, A.A. Adesina, R. Lange, Chem. Eng. Sci. 61 (2006) 2565–2573.
[45] M. Koike, D. Li, H. Watanabe, Y. Nakagawa, K. Tomishige, Appl. Catal. A—Gen. 506 (2015) 151–162.
[46] C. Wu, P.T. Williams, Appl. Catal. B—Environ. 96 (2010) 198–207.
[47] S. Helveg, J. Sehested, J.R. Rostrup-Nielsen, Catal. Today 178 (2011) 42–46.
[48] D.L. Trimm, Catal. Today 49 (1999) 3–10.
[49] C. Wu, P.T. Williams, App. Catal. B—Environ. 87 (2009) 152–161.
[50] A.G. Gayubo, J. Vicente, J. Ereña, L. Oar-Arteta, M.J. Azkoiti, M. Olazar, J. Bilbao, Appl. Catal. A—Gen. 483 (2014) 76–84.
[51] N. Latorre, F. Cazaña, V. Martínez-Hansen, C. Royo, E. Romeo, A. Monzón, Catal. Today 172 (2011) 143–151.